JOURNAL OF GUIDANCE, CONTROL, AND DYNAMICS
Vol. 20, No. 5, September–October 1997

On-Orbit Robust Control Experiment of Flexible Spacecraft ETS-VI

Takashi Kida* and Isao Yamaguchi†
National Aerospace Laboratory, Tokyo 182, Japan
Yuichi Chida‡
Toshiba Corporation, Kanagawa 210, Japan
and
Takeshi Sekiguchi§
National Space Development Agency, Ibaraki 305, Japan

An on-orbit attitude and vibration control experiment has been performed as a part of experiments of the ETS-VI, which was launched by the H-II rocket in August 1994. The purpose is to develop precise attitude control technology for future large spacecraft or large space structures. To this end, we have designed three types of controllers in linear quadratic Gaussian and H_∞ frameworks to achieve the robust stability against residual modes and modal parameter errors. The experiments were done at the beginning of 1995, and their feasibility has been proved. The flight experiment results and the modeling and the controller synthesis methods are reported. Based on the on-orbit results, the capabilities of controllers are compared and discussed.

Introduction

DURING the past two decades, the issues of modeling and control technologies of large space structures have been studied extensively, and many theoretical and experimental results have been reported. However, very few papers have appeared that discussed on-orbit experimental results using actual space structures or large free flyers, despite their obvious importance. Exceptions are the middeck active control experiment[1] and the Hubble space telescope pointing control study.[2]

With this motivation, since 1987 we have been developing a plan of an on-orbit control experiment using flexible spacecraft ETS-VI (Ref. 3), and the project was completed in 1995 (Ref. 4).

The ETS-VI, the sixth engineering test satellite, is a three-axis stabilized geosynchronous spacecraft with a pair of large lightweight solar panels, whose main mission is advanced communication experiments. A view of the ETS-VI is shown in Fig. 1. Controlling such a large flexible spacecraft within high accuracy requires control of its structural vibration. Vibration control, however, is a challenging technology for the following reasons. First, the structural vibration is described by a high-order modal equation. Mathematically, it has an infinite number of modes spread in the wide-frequency range. Second, accurate modal parameter identification is difficult in a 1-*g* ground environment. Third, the modal damping ratio is very small. Hence, in the worst case, lightly damped modes are easily excited by the controller, resulting in the spillover destabilization of the closed-loop system. One way to overcome these problems is to make a reduced-order model based on an accurately identified full-order model and to design a reduced-order controller with robust properties against the inevitable model uncertainties.

In view of this, the objective of our experiment is to establish the flexible spacecraft modeling and control technology and to demonstrate its capability in space. To this end, we have performed the following.

1) Before the launch, modal parameters of solar panels are estimated on the ground. The attitude controllers are designed based on the prelaunch model.

2) After the launch, the attitude control experiment is performed. Additionally, the spacecraft is excited in orbit, and modal parameters are identified based on the telemetry data.

3) Postflight analysis is performed to compare the flight data with the designed performance.

This paper describes the modeling method and the control law synthesis procedures for the on-orbit experiment. Then the experimental results are shown and analyzed.

Spacecraft System

The ETS-VI was launched by the National Space Development Agency of Japan using the H-II launch vehicle in August 1994. Although it was injected into an elliptic orbit because of the liquid apogee propulsion subsystem failure, its perigee was raised to a certain height by the orbit modification, which finally enables the three-axis attitude control. The final orbit is a 3-day regressive elliptic orbit of a 14-h period with 0.5 eccentricity and a 13.3-deg orbital inclination. The height of apogee is 38,640 km, and that of perigee is 8602 km. Then communication antennas were erected and directed to yaw direction, and solar panels were deployed in the pitch direction and made to rotate by paddle drive electronics (PDE) around the pitch axis, as shown in Fig. 2. The fully deployed spacecraft measures $30 \times 9.3 \times 7.8$ m, and its initial weight is about 2000 kg. The moments of inertia about the roll, pitch, and yaw axes are approximately 15,340, 5000, and 14,940 kgm^2, respectively, when the panel angle is 180 deg. After some housekeeping operations, the attitude control experiment was carried out around the apogee point, just as planned, for 16 days from December 1994 to July 1995.

The experiment makes use of the attitude control subsystem of ETS-VI and six paddle accelerometers (PACC) mounted on panels. The attitude angles and their rates are precisely estimated by the Kalman-filter-based attitude determination logic from the measurements of the Earth sensors assembly, inertial reference unit (IRU), and rate-integrated gyro assembly (RIGA). The accuracy of roll/yaw angles is 0.002 deg ($\pm 3\sigma$), and that of pitch is 0.012 deg ($\pm 3\sigma$). The degraded accuracy of pitch is due to the performance limitation of RIGA, whereas roll/yaw are estimated by using the high-performance tuned dry gyro of the IRU. Although the primary actuator of the bus controller is the reaction wheels, the reaction control system (RCS) having the maximum torque capability of

Received June 17, 1996; presented as Paper 96-3843 at the AIAA Guidance, Navigation, and Control Conference, San Diego, CA, July 29–31, 1996; revision received April 28, 1997; accepted for publication May 9, 1997.

*Senior Researcher, Space Technology Research Group; currently Professor, Department of Mechanical and Control Engineering, University of Electro-Communications, Chofugaoka, Chofu, Tokyo 182, Japan. Senior Member AIAA.

†Senior Researcher, Space Technology Research Group, Jindaiji-Higashi, Chofu. Member AIAA.

‡Research Scientist, R&D Center, Ukishima, Kawasaki.

§Engineer, Tsukuba Space Center, Sengen, Tsukuba.

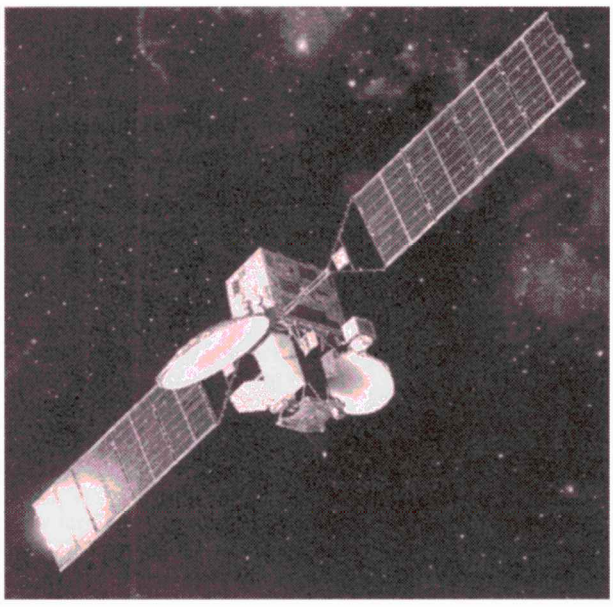

Fig. 1 Artist's view of ETS-VI.

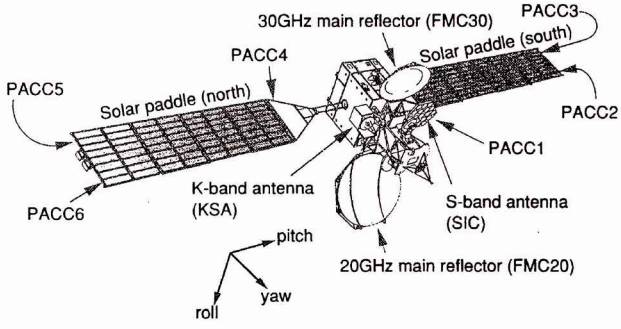

Fig. 2 Spacecraft system.

0.95 Nm is used for the experiment. The onboard control algorithms of the experiment are remotely loaded to the random access memory area of 2.6 Kbytes in the attitude control electronics (ACE) from the ground station and are executed by commands. The sampling rate of the closed-loop control is 4 Hz. During the control experiment, attitude angles, attitude rates, and control signals are monitored through the 1-Hz telemetry. Then they are transmitted to the engineering workstation for further analysis and the evaluation.

Modeling

The constraint-free modal equations of the solar panels of the north wing (N) and the south wing (S) are first obtained. The vibration of out-of-plane (OP) bending, in-plane (IP) bending, and torsion (TS) is described as

$$\ddot{\xi}_{i,k} + \Omega^2_{i,k}\xi_{i,k} = 0 \tag{1}$$

for $i =$ OP, TS, and IP and $k =$ N and S, where $\xi_{i,k}$ is the modal coordinate and $\Omega^2_{i,k}$ is the modal stiffness for the modal mass normalized unity. In the 1-g environment, the experimental modal analysis of the whole solar panel is not possible. Hence the modal parameters of each panel are mathematically computed in two ways. One is the finite element method (FEM), and the other is component modal synthesis (CMS) using measured modal data. For the CMS, the solar panel is divided into four substructures and the component modal test is conducted for several configurations.[5] By comparing these two results, the stiffness parameters of the solar cell membrane and the panel joints of the original FEM model are iteratively adjusted, until the resulting modal stiffness of Eq. (1) becomes a good approximation of the CMS result. Thus we have made prelaunch estimates. Then the equation of the spacecraft attached with a pair of panels is described in the body-fixed frame by the standard constrained modal equation[6]

$$J^b\ddot{\theta}^b + \Delta^b\ddot{\xi} = u^b, \qquad \ddot{\xi} + \Omega^2\xi + \Delta^{bT}\ddot{\theta}^b = 0 \tag{2}$$

where θ^b is the roll/pitch/yaw attitude angle and u^b is control torque. The global coordinates ξ and the stiffness matrix Ω are constructed as $\Omega = \text{diag}\{\Omega_{i,k}\}$ and $\xi = \text{col}\{\xi_{i,k}\}$ for all i and k. Because the solar panel rotates around the pitch axis at the orbital rate, the global vehicle inertia J^b and the coupling matrix Δ^b depend on the panel angle δ. For example, roll is coupled with OP bending and yaw with IP bending, when the panel angle is 90 or 270 deg. When the angle is 0 or 180 deg, the relation is reversed. The TS is coupled only with pitch, regardless of the panel angle. To make it the time-invariant system, we transform the equation into the panel frame. By the coordinate transformation $\theta^b = T(\delta)\theta^a$, where $T(\delta)$ is the direction cosine matrix from the body frame to the panel frame, Eq. (2) premultiplied by $T^T(\delta)$ becomes

$$J^a\ddot{\theta}^a + \Delta^a\ddot{\xi} = u^a, \qquad \ddot{\xi} + \Omega^2\xi + \Delta^{aT}\ddot{\theta}^a = 0 \tag{3}$$

where $J^a = T^TJ^bT$, $\Delta^a = T^T\Delta^b$, and $u^a = T^Tu^b$. Because the inertia around the roll/yaw axes of the central rigid body of the ETS-VI is symmetrical, matrices J^a and Δ^a become independent from δ and block diagonal, $J^a = \text{block-diag}\{J^a_i\}$ and $\Delta^a = \text{block-diag}\{\Delta^a_i\}$. Therefore Eq. (3) is decoupled into the $i =$ OP, TS, IP direction. Solving a generalized eigenvalue problem for each i direction and adding the modal damping term yield an unconstrained modal equation,

$$\ddot{\eta}_i + 2\zeta_i\Sigma_i\dot{\eta}_i + \Sigma^2_i\eta_i = \Phi^T_i u^a_i \tag{4}$$

where Φ_i is the modal shape at the rigid body, $\Sigma^2_i \geq 0$ is modal stiffness, and $2\zeta_i\Sigma_i \geq 0$ is modal damping. The modal damping ratio ζ_i is assumed to be 0.005 for all i. Thus we obtain a prelaunch design model.

Besides this, the on-orbit identification is performed after the launch. For this purpose, the spacecraft is vibrated by RCS with the pseudorandom and the impulse signals. Figure 3 shows the telemetry data of roll, roll-rate, and the panel acceleration measured by PACC when a spacecraft is excited with the pulse of 0.3(s) width (left) and with the M-sequence pseudorandom (right) by holding the panel angle at 180 deg.

From the obtained attitude angle/rate and the panel acceleration signals, we make an evaluation model by identification algorithms, such as MEM, FFT, ARX, ERA, and the subspace method.[7,8] Table 1 compares the modal frequencies of the prelaunch design model and the on-orbit evaluation model. Considerable differences are observed, mainly due to the difficulty of the component modal test under 1 g, even though it is performed for smaller substructures. The numerical errors at calculating CMS and solving the eigenvalue

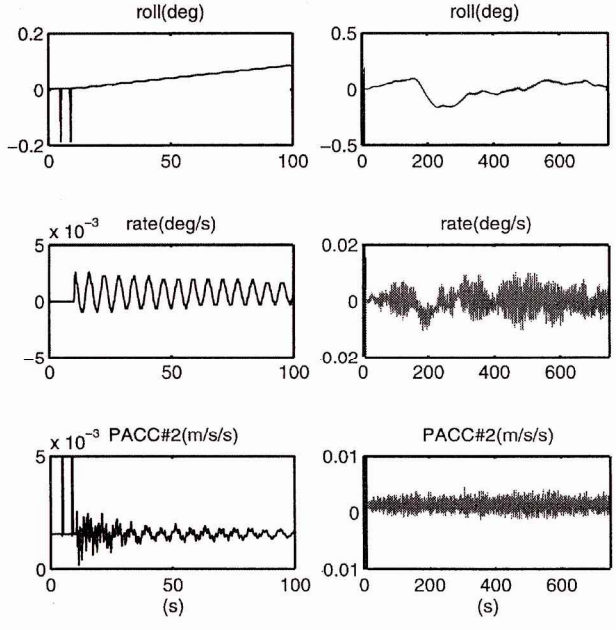

Fig. 3 Open-loop time response to impulse (left) and pseudorandom (right) input.

problem are considered secondary. Among the modes in Table 1, we need only the controllable, observable modes, which are asymmetric modes coupled with the attitude motion, for the controller design.

Because of the schedule constraint and the safety of the experiment, all controllers have been designed based on the design model and evaluated in various ways before the launch.

The measurements available for the control experiment are the roll/pitch/yaw angles and their rates estimated by the attitude determination logic. They are in the panel-fixed frame

$$y_i^{1a} = \Phi_i \eta_i, \qquad y_i^{2a} = \Phi_i \dot{\eta}_i \tag{5}$$

The transfer function from u_i to $y_i^a = [y_i^{1a} \;\; y_i^{2a}]^T$ is

$$y_i^a = P_i^a(s) u_i^a \tag{6}$$

where $P_i^a(s) = \Phi_i (Is^2 + 2\zeta_i \Sigma_i s + \Sigma_i^2)^{-1} \Phi_i^T$, whose state-space equation is shown in the Appendix. This is the full-order model finally obtained in the modeling phase.

Control Law

To design a reduced-order controller, we make a reduced-order model

$$y_i^a = Q_i^a(s) u_i^a \tag{7}$$

from the full-order model $y_i = P_i(s) u_i$ based on the design model parameters. The parameters of $Q_i^a(s)$ of OP and IP are shown in the Appendix. Those of TS are omitted. We determine the reduced-order model of OP, IP, and TS as follows. The OP reduced-order model is the rigid mode and the first vibration mode. The IP first mode is rejected from the reduced-order model because its frequency is critical for implementing the reliable controller. The order of the reduced-order model is determined from the control bandwidth limited by the ACE/CPU sampling rate (4 Hz). For example, the first OP is included because its modal frequency is one decade smaller than the Nyquist frequency. At the frequency range, the phase delay caused by sampling is negligible. The second OP frequency, a quarter of the Nyquist frequency, is not considered sufficiently small. Therefore it is treated as residual. The effect of TS vibration is negligibly small. Therefore TS motion can be regarded as a rigid body. The reduced-order controller is then designed for $i =$ OP, TS, IP:

$$u_i^a = C_i^a(s) y_i^a \tag{8}$$

Table 1 Modal frequencies, Hz

No.	Modal name[a]	Design model	Evaluation model
1	1st OS	0.106	0.092
2	1st OA	0.185	0.162
3	1st IS	0.264	0.229
4	1st TS	0.395	0.395
5	1st TA	0.399	0.399
6	1st IA	0.505	0.457
7	2nd OS	0.539	0.673
8	2nd OA	0.552	0.673
9	2nd TS	1.260	1.28
10	2nd TA	1.261	1.36
11	3rd OS	1.434	1.64
12	3rd OA	1.438	1.72
13	2nd IS	2.885	3.95
14	2nd IA	2.890	3.96

[a]O, out-of-plane bending; I, in-plane bending; T, torsion; A, asymmetric modes; and S, symmetric modes.

such that it achieves the robust stability against the residual modes and the parameter errors. Thus the triplet of the reduced-order controllers for OP, TS, and IP is obtained. We employed the following three controller synthesis methods: 1) a linear quadratic Gaussian (LQG) controller having frequency-shaping capability, 2) an H_∞ controller by the robust stability-degree assignment method, and 3) an H_∞ controller with direct velocity feedback.

All of the controllers are designed using linear controller synthesis computer-aided design (CAD) and then discretized according to the sampling rate of 4 Hz. For the implementation, the discrete-time control inputs are transformed back to the body frame and quantized by a pseudorate modulator. Then they are converted into the signals to the valve drive electronics of RCS thrusters. The block diagram of the control system is shown in Fig. 4. In the following, the synthesis procedures are outlined, and design results are shown. The state-space realization of the obtained controllers is summarized in the Appendix. The subscript i and the superscript a are dropped hereafter.

LQG Controller

The standard linear quadratic regulator (LQR) is considered to have robustness in the sense that it leads the phase of the loop transfer function to -90 deg (Ref. 9). However, the property is not suitable for the vibration control because the unmodeled residual modes exist in the high-frequency range. We consider the optimal regulator that minimizes the following frequency-dependent cost so that the control input does not include the high-frequency signals[10,11]:

$$\frac{1}{2\pi} \int_{-\infty}^{+\infty} \|z_1(j\omega)\|^2 + \rho^2 \|r(j\omega) u(j\omega)\|^2 \, \mathrm{d}\omega \tag{9}$$

where ρ is the positive scalar tradeoff parameter and z_1 is the control variable. Because our concern lies in attitude control, z_1 is set as $z_1 = y^1$. The frequency-dependent weight $r(s)$ is selected as $r^{-1}(s) = \omega_0^2/(s^2 + 2\zeta_0\omega_0 s + \omega_0^2)$ such that $r^{-1}(0) = 1$ and $r^{-1}(\infty) = 0$. The resulting optimal regulator gain is a stable, proper, rational function that preserves the low-pass property of $r^{-1}(s)$. By using the frequency-dependent LQR with the state estimator, we obtain the output feedback controller $u = C(s)y$, which gives the magnitude of the loop transfer function $C(j\omega)Q(j\omega)$ the high roll-off rate in the high-frequency region. By utilizing the property, the frequency-shaped LQG controller has the robustness against the residual modes. We solve the problem by converting it into an equivalent H_2 problem as follows.[12] Suppose an extended system driven by a fictitious control input v weighted as $u = r^{-1}(s)v$,

$$\begin{aligned} y &= Q_r(s)v + Q(s)w_1 + \mu w_2 \\ z_1 &= V Q_r(s)v + V Q(s)w_1, \qquad z_2 = \rho v \end{aligned} \tag{10}$$

where $Q_r(s) = Q(s)r^{-1}(s)$, $V = [1 \;\; 0]$, and w_1 and w_2 are Gaussian white noise processes with unit intensities. Find a controller $v = C_v(s)y$ to minimize the expected value of the cost

$$\frac{1}{2\pi} \int_{-\infty}^{+\infty} \|z(j\omega)\|^2 \, \mathrm{d}\omega \tag{11}$$

subject to Eq. (10), where $z = [z_1 \;\; z_2]^T$. The closed-loop transfer function $F(s)$ from $w = [w_1 \;\; w_2]^T$ to z is, from Eq. (10),

$$z = F(s)w, \qquad F = \begin{bmatrix} VSQ & \mu VT \\ \rho C_v SQ & \rho\mu C_v S \end{bmatrix} \tag{12}$$

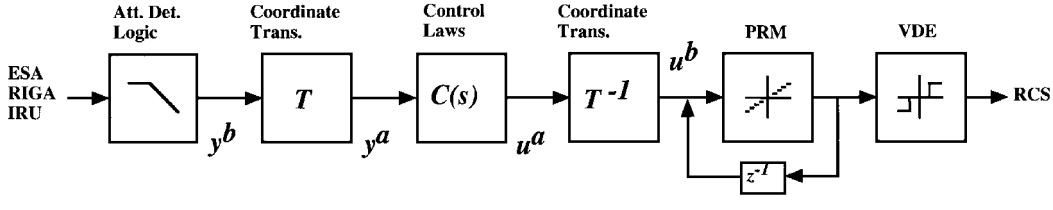

Fig. 4 Block diagram of spacecraft control system.

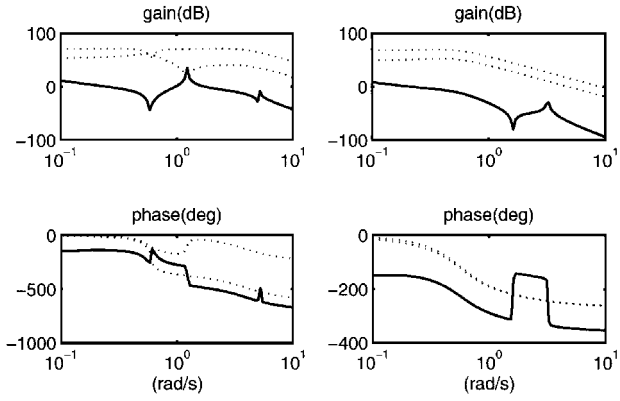

Fig. 5 Design A of OP (left) and IP (right) controllers; Bode plots: ——, $C(j\omega)P(j\omega)$ and ·····, $C(j\omega)$.

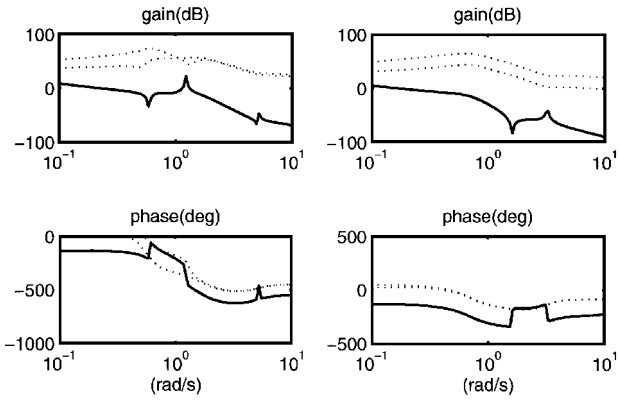

Fig. 6 Design B of OP (left) and IP (right) controllers; Bode plots: ——, $C(j\omega)P(j\omega)$ and ·····, $C(j\omega)$.

which is the strictly proper transfer function, where $S=(I-Q_rC_v)^{-1}$ and $T=(I-Q_rC_v)^{-1}Q_rC_v$. Substituting Eq. (12) into Eq. (11) yields

$$\frac{1}{2\pi}\int_{-\infty}^{+\infty}\mathrm{tr}(FF^H)\,\mathrm{d}\omega \tag{13}$$

The H_2 optimal controller $v=C_v(s)y$ minimizing Eq. (13) yields $u=r^{-1}(s)C_v(s)y$.

In Fig. 5, the design results of OP (left) and IP (right) controllers are shown by Bode plots of the loop transfer function $C(j\omega)P(j\omega)$ (solid line) and the transfer function of $C(j\omega)$ (dotted line). The OP controller stabilizes the first mode by the phase margin and the second mode by the gain margin. The former is the phase stabilization, and the latter is the gain stabilization.[13] By the IP controller, all of the vibration modes are gain stabilized. Therefore, the cutoff frequency of the OP controller is higher than that of the IP controller. The design result of the TS controller is omitted in this paper.

H_∞ Controller

The H_∞ design approach enables the issue of robustness against residual modes to be directly addressed.[14] However, the problem can be ill-conditioned when the spacecraft has the lightly damped vibration modes and the undamped rigid modes. Accordingly, it does not work sufficiently in its original form. Having this in mind, we consider the two-block, mixed-sensitivity H_∞ problem in two ways.

Robust Stability-Degree Assignment

For the measurement y and the control variable z_1,

$$y=P(s)u, \qquad z_1=\gamma^{-1}Vy \tag{14}$$

we define the reduced-order model $y=Q(s)u$ as

$$P=Q(s)+R(s), \qquad R(s)=\Delta_r(s)W(s), \qquad \|\Delta_r\|_\infty\le 1 \tag{15}$$

where $W(s)$ is a stable proper rational $W(s)=(a_0s^2+a_1s+a_2)/(s^2+b_1s+b_2)$ with $W(\infty)\neq 0$. We consider the following extended system:

$$\begin{aligned} y&=Q(s)u+w\\ z_1&=\gamma^{-1}VQ(s)u+\gamma^{-1}Vw, \qquad z_2=W(s)u \end{aligned} \tag{16}$$

where z_2 and w are the fictitious output and input, respectively. The linear fractional transform of Eq. (16) and $w=\Delta_r z_2$ are equivalent to Eq. (14). Substitution of $u=C(s)y$ into Eq. (16) yields the following closed-loop system:

$$z_1=\gamma^{-1}VS(s)w, \qquad z_2=W(s)T'(s)w \tag{17}$$

where $S=(I-QC)^{-1}$ and $T'=C(I-QC)^{-1}$. The closed-loop system has the robust stability against the residual modes when $\|WT'\|_\infty<1$, and it has the disturbance rejection capability of γ when $\|VS\|_\infty<\gamma$. To satisfy these two requirements, we obtain the controller that satisfies the sufficient condition

$$\|M\|_\infty<1, \qquad M=\begin{bmatrix}\gamma^{-1}VS\\ WT'\end{bmatrix} \tag{18}$$

We solve the problem by the standard state-space algorithm.[15,16] However, Eq. (16) does not satisfy the solvability condition because $Q(s)$ has poles at the origin of the s plane. Hence, the robust stability degree assignment method is employed.[17] First, we map the plant (16) from the s plane to the $\tilde{s}$ plane by the transform $s=\tilde{s}-\alpha$, where α is a positive scalar. Then we obtain the controller $\tilde{C}(\tilde{s})$ that satisfies

$$\|\tilde{M}\|_\infty<1 \tag{19}$$

Mapping $\tilde{C}(\tilde{s})$ back to the s plane by the inverse transform $\tilde{s}=s+\alpha$ yields $C(s)$. Because Eq. (19) is the sufficient condition of Eq. (18), the resulting controller $C(s)$ satisfies the original robust condition.[18] Additionally, the closed-loop poles have the stability margins corresponding to α.

Figure 6 shows the Bode plots of the transfer function of the obtained controllers (dotted line) and the loop transfer functions (solid line) of OP (left) and IP (right). Qualitatively, the controllers have the same frequency properties as design A.

Damping Enhancement by Feedback

For the measurement y and the control variable z_1,

$$y=P(s)u, \qquad z_1=\gamma^{-1}Vy \tag{20}$$

we consider another set of the mixed-sensitivity problem by defining $y=Q(s)u$ as

$$\begin{aligned} P(s)&=Q(s)[I+R(s)]\\ R(s)&=\Delta_r(s)W(s), \qquad |\Delta_r|\le 1\ \forall\omega \end{aligned} \tag{21}$$

The generalized plant is, in this turn,

$$y=Q(s)(u+w), \qquad z_1=\gamma^{-1}VQ(s)(u+w), \qquad z_2=W(s)u \tag{22}$$

The linear fractional transform with $w=\Delta_r z_2$ is equivalent to Eq. (20). Given the controller $u=C(s)y$, the closed-loop system of Eq. (22) becomes

$$z_1=\gamma^{-1}VQ(s)S(s)w, \qquad z_2=W(s)T(s)w \tag{23}$$

where $S=(I-CQ)^{-1}$ and $T=CQ(I-CQ)^{-1}$. The closed-loop system is robustly stable when $|WT|<1\ \forall\omega$. The disturbance is attenuated by the amount of γ when $|VQS|<\gamma\ \forall\omega$. To satisfy these conditions, we design a controller satisfying

$$\|M\|_\infty<1, \qquad M=\begin{bmatrix}\gamma^{-1}VQS\\ WT\end{bmatrix} \tag{24}$$

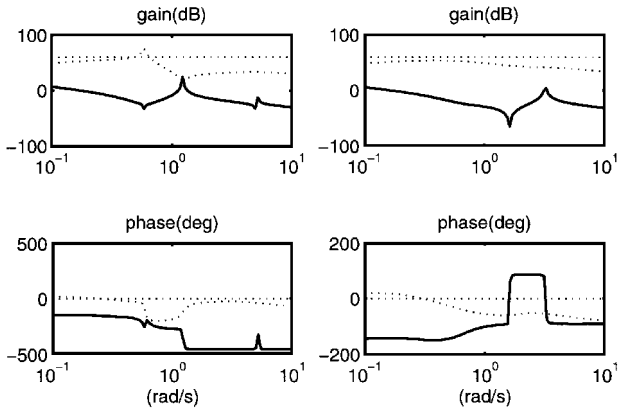

Fig. 7 Design C of OP (left) and IP (right) controllers; Bode plots: ——, $C(j\omega)P(j\omega)$ and ·····, $C(j\omega)$.

However, the standard algorithm does not solve the problem because $Q(\infty) = 0$. Hence, we modify Eq. (22) as $y = Q(s)u + Q(s)w + \epsilon v$ by introducing a fictitious input v with negligibly small ϵ. Although $Q(s)$ has poles at the origin of the s plane, this is not the problem in the case, because the weighting function of $S(s)$ is $Q(s)$ itself.

Generally, it is known that the H_∞ controller from the weighted mixed-sensitivity problem formulation always cancels the stable poles of the plant with its transmission zeros. The stable poles are, in our problem, the slightly damped vibration modes that have the parameter estimation errors as mentioned earlier. Therefore, the imperfect pole-zero cancellation occurs near the imaginary axis in the complex plane. This fact could violate the closed-loop internal stability in the worst case. To avoid this, the collocated rate feedback is employed to enhance the modal damping.[19,20] By decomposing the control input u into $u = u^1 + u^2$, we first apply the minor control loop of the angular rate feedback $u^2 = -Dy^2$ to Eq. (4). The closed-loop system becomes

$$\ddot{\eta} + (2\zeta\Sigma + \Phi^T D\Phi)\dot{\eta} + \Sigma^2\eta = \Phi^T u^1 \tag{25}$$

where $2\zeta\Sigma + \Phi^T D\Phi$ is positive definite if $2\zeta\Sigma \geq 0$ and $D > 0$ when (Σ, Φ^T) is stabilizable.[21] By increasing D, the energy dissipation of the plant is increased, preserving the symmetry property of $P(s)$, which means the collocated rate feedback is structurally robust. Then the solution of the mixed-sensitivity problem for the reduced-order model of the damping-enhanced new plant (25) gives $u^2 = C^2(s)y$. Because the plant has the ample stability margin, the internal stability is guaranteed even when the imperfect pole-zero cancellation occurs.

Design results are shown in Fig. 7. The OP controller stabilizes the rigid and the first bending modes by the phase stabilization, and the second mode is by the amplitude stabilization. This is the similar result as designs A and B. However, the first IP residual mode is stabilized by leading phase. This is the effect of the collocated rate feedback control.

Prelaunch Evaluation

The sensitivity analysis to the model errors has been made extensively by linear CAD. Besides, we have made the following steps to evaluate the nonlinearity effects of spacecraft: 1) an air/table experiment—the control experiment is performed by using an ETS-VI miniature model mounted on the single-axis air bearing; 2) a static closed-loop test—a setup of the ETS-VI dynamics simulator linked to the ACE engineering model is used to examine the onboard control logic; 3) a simulation—a numerical simulation is made to evaluate the effects of nonlinear components; and 4) an emulation—emulation of the ACE is made to evaluate onboard software of machine language.

Each evaluation step has played its own role. Various improvements in algorithms and experiment sequences have been achieved.

Results of the On-Orbit Experiment

The control experiment has been performed by holding the panel rotation at the angle of 270 or 180 deg according to the experiment date to avoid the unknown disturbance torque caused by PDE. The initialization of the system and wheel unloading are made while the bus controller is in operation. Then the control logic is changed to the algorithm of the control experiment from that of the bus control. After confirming the closed-loop stability, we obtain the step response to the attitude command and the impulse response to the disturbance torque generated by 1-s thrusting of the RCS to evaluate the controller performance.

The experiment of controller A was performed in the configuration of the 270-deg panel angle in January 1995. In that case, the OP controller controls roll attitude, and the IP controller controls yaw attitude. In Fig. 8, the experiment's results of impulse disturbance responses of roll, roll-rate, and roll-torque command (left) and yaw, yaw-rate, and yaw-torque command (right) are shown by thick lines, compared with the responses estimated at the design phase (thin lines). The robust stability and the disturbance rejection capability are verified. Additionally, by comparing responses of roll rate and yaw rate, it is observed that the wide-range OP controller is more effective than the narrow-range IP controller in the disturbance rejection capability. This is because the OP controller controls the

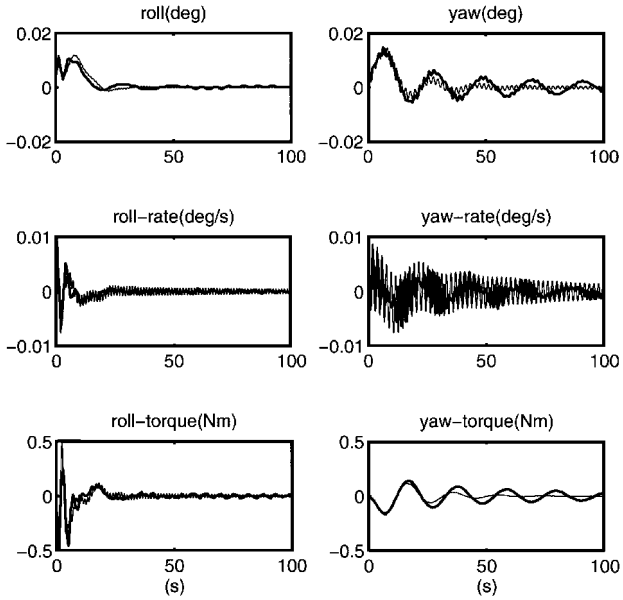

Fig. 8 Design A impulse disturbance responses of roll (left) and yaw (right): ——, experimental results and ——, design results.

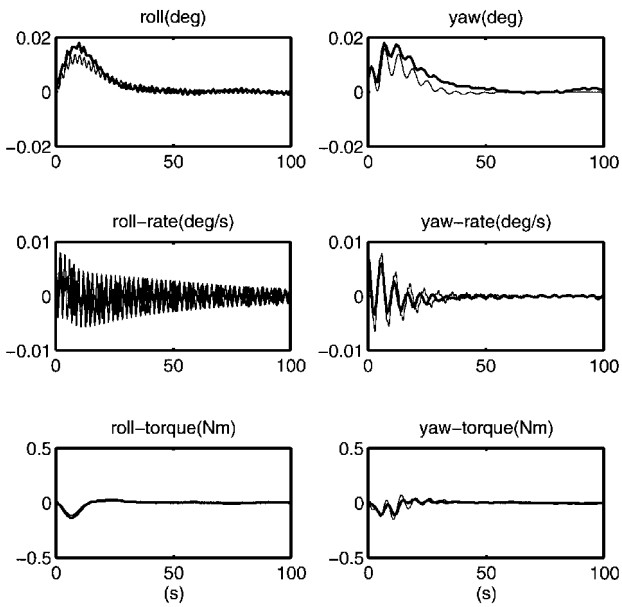

Fig. 9 Design B impulse disturbance responses of roll (left) and yaw (right): ——, experimental results and ——, design results.

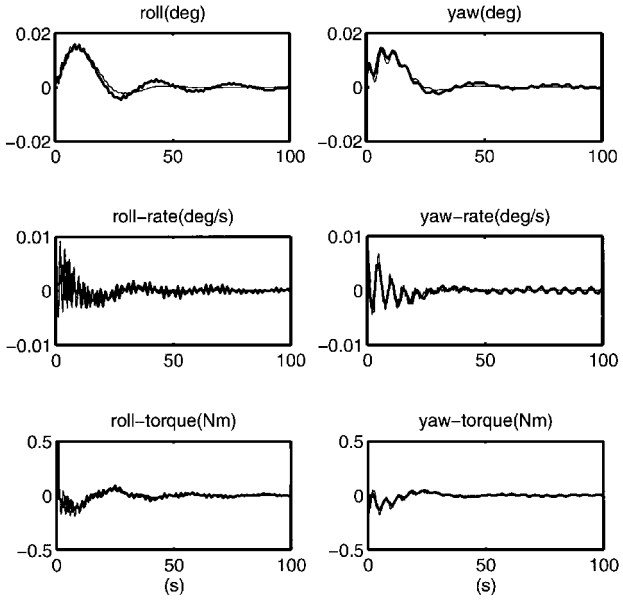

Fig. 10 Design C impulse disturbance responses of roll (left) and yaw (right): ——, experimental results and ——, design results.

first mode, whereas the IP controller does not. The decay of yaw rate is the effect of natural damping.

The results of design B are shown in Fig. 9, and those of design C are shown in Fig. 10. These two experiments were done in March 1995, after the eclipse in February, by holding the solar panel at the angle of 180 deg. In this case, the OP controller is coupled with yaw and the IP controller with roll. The disturbance rejection capabilities of yaw responses are better than those of roll in design B. This is for the same reason as in the case of design A. However, these capabilities of OP and IP are comparable in design C. This is because the IP controller bandwidth is widened, as shown in Fig. 7, by the assistance of the collocated rate feedback, although the higher-frequency modes are residual modes.

On the modal parameter errors, slight differences between experimental and design responses are observed in Figs. 8–10. However, they are not fatal for the spacecraft mission.

Discussion and Conclusion

Through the on-orbit experiment, we have confirmed the feasibility of the robust controller. This is what we intended, although the controllers are not so much new algorithms as standard synthesis methods. From the results, we expect to learn lessons available for developing future large space structures' control technology.

Regarding the comparison of the three methods, the following points are added. The LQG controller (design A) has shown an excellent performance. However, it is obtained through laborious iterations of tuning many parameters and evaluating closed-loop time and frequency responses by CAD, without systematic procedure, because the robust stability theorem is not directly applied to the H_2 synthesis. The H_∞ synthesis guarantees the robust stability, once the weighting function is determined. However, the robustness against parameter errors should be discussed. In designs B and C, we have attempted to cope with the problem by giving closed-loop poles ample stability margin. The stability degree assignment method (design B) is efficient for the purpose. However, the achieved stability margin is limited because the excessively large α makes the generalized plant unstabilizable. The design is performed by tuning two parameters, α and γ. Finally, the direct velocity feedback (design C) is another option giving closed-loop stability margin. It has a structural robustness in itself and a potential capability to lead the phase in the higher-frequency range of residual modes. This is recommended when rate measurements are available.

Besides these robust optimal controllers, we have prepared a classical proportional-derivative controller, which has the simplest structure, for an on-orbit experiment. It has been expected to achieve a certain performance for single-input and single-output space structures. However, we regret that it was omitted from the experiment because of the schedule limitation.

Appendix: Models of Spacecraft and Controllers

We describe the state-space minimal realization of a transfer function matrix $G(s) = C(sI - A)^{-1}B + D$ as

$$G(s) = \left[\begin{array}{c|c} A & B \\ \hline C & D \end{array}\right]$$

Then the state-space equations of full-order prelaunch models of $P^a_{\mathrm{OP}}(s)$ and $P^a_{\mathrm{IP}}(s)$ are

$$\left[\begin{array}{cccccccc|c}
0.00e^{+0} & 0.00e^{+0} & 0.00e^{+0} & 0.00e^{+0} & 1.00e^{+0} & 0.00e^{+0} & 0.00e^{+0} & 0.00e^{+0} & 0.00e^{+0} \\
0.00e^{+0} & 0.00e^{+0} & 0.00e^{+0} & 0.00e^{+0} & 0.00e^{+0} & 1.00e^{+0} & 0.00e^{+0} & 0.00e^{+0} & 0.00e^{+0} \\
0.00e^{+0} & 0.00e^{+0} & 0.00e^{+0} & 0.00e^{+0} & 0.00e^{+0} & 0.00e^{+0} & 1.00e^{+0} & 0.00e^{+0} & 0.00e^{+0} \\
0.00e^{+0} & 0.00e^{+0} & 0.00e^{+0} & 0.00e^{+0} & 0.00e^{+0} & 0.00e^{+0} & 0.00e^{+0} & 1.00e^{+0} & 0.00e^{+0} \\
0.00e^{+0} & 0.00e^{+0} & 0.00e^{+0} & 0.00e^{+0} & 0.00e^{+0} & 0.00e^{+0} & 0.00e^{+0} & 0.00e^{+0} & 7.99e^{-3} \\
0.00e^{+0} & -1.52e^{+0} & 0.00e^{+0} & 0.00e^{+0} & 0.00e^{+0} & -1.23e^{-2} & 0.00e^{+0} & 0.00e^{+0} & -1.46e^{-2} \\
0.00e^{+0} & 0.00e^{+0} & -2.75e^{+1} & 0.00e^{+0} & 0.00e^{+0} & 0.00e^{+0} & -5.24e^{-2} & 0.00e^{+0} & -4.45e^{-3} \\
0.00e^{+0} & 0.00e^{+0} & 0.00e^{+0} & -1.90e^{+2} & 0.00e^{+0} & 0.00e^{+0} & 0.00e^{+0} & -1.38e^{-1} & 1.93e^{-3} \\
\hline
-7.99e^{-3} & -1.46e^{-2} & -4.45e^{-3} & 1.93e^{-3} & 0.00e^{+0} & 0.00e^{+0} & 0.00e^{+0} & 0.00e^{+0} & 0.00e^{+0} \\
0.00e^{+0} & 0.00e^{+0} & 0.00e^{+0} & 0.00e^{+0} & -7.99e^{-3} & -1.46e^{-2} & -4.45e^{-3} & 1.93e^{-3} & 0.00e^{+0}
\end{array}\right]$$

and

$$\left[\begin{array}{ccccccc|c}
0.00e^{+0} & 0.00e^{+0} & 0.00e^{+0} & 1.00e^{+0} & 0.00e^{+0} & 0.00e^{+0} & 0.00e^{+0} \\
0.00e^{+0} & 0.00e^{+0} & 0.00e^{+0} & 0.00e^{+0} & 1.00e^{+0} & 0.00e^{+0} & 0.00e^{+0} \\
0.00e^{+0} & 0.00e^{+0} & 0.00e^{+0} & 0.00e^{+0} & 0.00e^{+0} & 1.00e^{+0} & 0.00e^{+0} \\
0.00e^{+0} & 0.00e^{+0} & 0.00e^{+0} & 0.00e^{+0} & 0.00e^{+0} & 0.00e^{+0} & -7.86e^{-3} \\
0.00e^{+0} & -1.04e^{+1} & 0.00e^{+0} & 0.00e^{+0} & -3.22e^{-2} & 0.00e^{+0} & 1.35e^{-2} \\
0.00e^{+0} & 0.00e^{+0} & -3.19e^{+2} & 0.00e^{+0} & 0.00e^{+0} & -1.79e^{-1} & 1.77e^{-3} \\
\hline
-7.86e^{-3} & 1.35e^{-2} & 1.77e^{-3} & 0.00e^{+0} & 0.00e^{+0} & 0.00e^{+0} & 0.00e^{+0} \\
0.00e^{+0} & 0.00e^{+0} & 0.00e^{+0} & -7.86e^{-3} & 1.35e^{-2} & 1.77e^{-3} & 0.00e^{+0}
\end{array}\right]$$

respectively. The reduced-order models are made from them, yielding $Q^a_{\mathrm{OP}}(s)$ and $Q^a_{\mathrm{IP}}(s)$:

$$\left[\begin{array}{ccccc|c} 0.00e^{+0} & 0.00e^{+0} & 1.00e^{+0} & 0.00e^{+0} & 0.00e^{+0} \\ 0.00e^{+0} & 0.00e^{+0} & 0.00e^{+0} & 1.00e^{+0} & 0.00e^{+0} \\ 0.00e^{+0} & 0.00e^{+0} & 0.00e^{+0} & 0.00e^{+0} & -7.99e^{-3} \\ 0.00e^{+0} & -1.52e^{+0} & 0.00e^{+0} & -1.23e^{-2} & -1.46e^{-2} \\ \hline -7.99e^{-3} & -1.46e^{-2} & 0.00e^{+0} & 0.00e^{+0} & 0.00e^{+0} \\ 0.00e^{+0} & 0.00e^{+0} & -7.99e^{-3} & -1.46e^{-2} & 0.00e^{+0} \end{array}\right],$$

$$\left[\begin{array}{cc|c} 0.00e^{+0} & 1.00e^{+0} & 0.00e^{+0} \\ 0.00e^{+0} & 0.00e^{+0} & -7.86e^{-3} \\ \hline -7.86e^{-3} & 0.00e^{+0} & 0.00e^{+0} \\ 0.00e^{+0} & -7.86e^{-3} & 0.00e^{+0} \end{array}\right]$$

The state-space equation of OP is fourth order and that of IP is second order with single input and two outputs. These are controllable and observable. All controllers are designed based on the equations with second-order weighting functions. First, LQG controllers of design A are

$$\left[\begin{array}{cccccc|cc} 0.00e^{+0} & 1.00e^{+0} & 0.00e^{+0} & 0.00e^{+0} & 0.00e^{+0} & 0.00e^{+0} & 0.00e^{+0} & 0.00e^{+0} \\ -1.72e^{+1} & -5.86e^{+0} & 1.01e^{+2} & 1.79e^{+1} & 6.63e^{+2} & 1.29e^{+3} & 0.00e^{+0} & 0.00e^{+0} \\ 0.00e^{+0} & 0.00e^{+0} & -2.63e^{-1} & -4.80e^{-1} & 3.50e^{-1} & -1.19e^{+0} & -3.29e^{+1} & -8.14e^{+1} \\ 0.00e^{+0} & 0.00e^{+0} & -2.15e^{-2} & -3.92e^{-2} & -2.88e^{-2} & 9.47e^{-1} & -2.69e^{+0} & -3.60e^{+0} \\ 7.99e^{-3} & 0.00e^{+0} & -6.00e^{-2} & -1.10e^{-1} & -6.10e^{-1} & -1.11e^{+0} & -7.51e^{+0} & -7.63e^{+1} \\ -1.46e^{-2} & 0.00e^{+0} & -5.63e^{-3} & -1.53e^{+0} & -1.16e^{+0} & -2.12e^{+0} & -7.04e^{-1} & -1.45e^{+2} \\ \hline -1.00e^{+0} & 0.00e^{+0} & 0.00e^{+0} & 0.00e^{+0} & 0.00e^{+0} & 0.00e^{+0} & 0.00e^{+0} & 0.00e^{+0} \end{array}\right]$$

and

$$\left[\begin{array}{ccccc|cc} 0.00e^{+0} & 1.00e^{+0} & 0.00e^{+0} & 0.00e^{+0} & 0.00e^{+0} & 0.00e^{+0} \\ -3.18e^{-1} & -7.96e^{-1} & 9.94e^{-1} & 9.18e^{+0} & 0.00e^{+0} & 0.00e^{+0} \\ 0.00e^{+0} & 0.00e^{+0} & -2.98e^{-1} & 3.39e^{-1} & -3.79e^{+1} & -8.42e^{+1} \\ -7.86e^{-3} & 0.00e^{+0} & -6.61e^{-2} & -5.81e^{-1} & -8.42e^{+0} & -7.39e^{+1} \\ \hline -1.00e^{+0} & 0.00e^{+0} & 0.00e^{+0} & 0.00e^{+0} & 0.00e^{+0} & 0.00e^{+0} \end{array}\right]$$

The H_∞ controllers of stability degree assignment (design B) yield the following:

$$\left[\begin{array}{cccccc|cc} -6.48e^{-1} & 1.06e^{+0} & -4.40e^{+0} & 3.16e^{+1} & -1.58e^{+1} & 6.18e^{+1} & -2.09e^{-7} & -2.92e^{-7} \\ -5.36e^{-1} & -3.66e^{-1} & 5.32e^{+0} & -3.81e^{+1} & 1.91e^{+1} & -7.47e^{+1} & -7.96e^{-6} & 3.05e^{-5} \\ -1.30e^{-2} & -2.09e^{-2} & -3.81e^{-1} & 2.10e^{+0} & -1.00e^{+0} & 4.09e^{+0} & -1.37e^{-2} & 1.28e^{-1} \\ -6.57e^{-3} & 9.79e^{-3} & -7.64e^{-2} & -4.43e^{-1} & 1.25e^{+0} & -9.00e^{-1} & 8.13e^{-1} & 3.75e^{-1} \\ -5.03e^{-3} & -1.06e^{-2} & -5.84e^{-2} & -5.74e^{-1} & -8.13e^{-1} & 1.73e^{+0} & -6.63e^{-1} & 1.16e^{+0} \\ 3.91e^{-3} & -2.79e^{-3} & -1.34e^{-1} & 3.34e^{-1} & -2.17e^{-1} & -1.44e^{+0} & -2.76e^{+0} & -1.37e^{+0} \\ \hline -1.65e^{+1} & -1.69e^{+1} & -7.10e^{+0} & 5.09e^{+1} & -2.55e^{+1} & 9.96e^{+1} & 0.00e^{+0} & 0.00e^{+0} \end{array}\right]$$

$$\left[\begin{array}{ccccc|cc} -3.72e^{-1} & 6.43e^{-1} & -6.17e^{-1} & 1.19e^{+1} & -1.65e^{-6} & 2.37e^{-5} \\ -1.83e^{-1} & -2.77e^{-1} & 2.57e^{+0} & -4.97e^{+1} & -1.17e^{-5} & 1.56e^{-4} \\ -1.17e^{-2} & -2.65e^{-2} & -3.60e^{-1} & 5.86e^{+0} & -9.55e^{-3} & 1.16e^{-1} \\ 3.62e^{-4} & -6.24e^{-3} & -1.34e^{-1} & -1.23e^{+0} & -3.23e^{+0} & -2.65e^{-1} \\ \hline -9.88e^{+0} & -3.03e^{+0} & -1.82e^{+0} & 3.53e^{+1} & 0.00e^{+0} & 0.00e^{+0} \end{array}\right]$$

for OP and IP, respectively. Finally, H_∞ controllers with direct velocity feedback (design C) are obtained as follows:

$$\left[\begin{array}{cccccc|cc} 2.74e^{+0} & 1.71e^{+1} & -4.11e^{+0} & -3.34e^{+0} & -5.41e^{-1} & 3.32e^{-1} & -2.78e^{+3} & 0.00e^{+0} \\ -2.45e^{+0} & -7.62e^{+0} & 2.00e^{+0} & 1.65e^{+0} & 2.47e^{-1} & -1.52e^{-1} & 1.32e^{+3} & 0.00e^{+0} \\ 2.28e^{-1} & 1.25e^{+0} & -4.25e^{-1} & -3.45e^{-1} & 3.47e^{-1} & -5.99e^{-4} & -2.24e^{+2} & 0.00e^{+0} \\ -1.97e^{-1} & -9.65e^{-1} & 3.03e^{-1} & 3.12e^{-2} & -5.12e^{-2} & -2.22e^{-1} & 1.69e^{+2} & 0.00e^{+0} \\ 4.20e^{+0} & 2.32e^{+1} & -6.08e^{+0} & -5.02e^{+0} & -8.24e^{-1} & 2.25e^{-1} & -4.09e^{+3} & 0.00e^{+0} \\ -1.36e^{+1} & -7.50e^{+1} & 1.95e^{+1} & 1.62e^{+1} & 2.43e^{+0} & -1.67e^{+0} & 1.32e^{+4} & 0.00e^{+0} \\ \hline 8.28e^{-3} & 1.30e^{-2} & 6.73e^{-1} & -6.12e^{-1} & 3.59e^{-1} & 1.08e^{-1} & 0.00e^{+0} & -1.00e^{+3} \end{array}\right]$$

and

$$\left[\begin{array}{ccccc|cc} -1.72e^{+0} & -2.50e^{-1} & -2.01e^{-1} & -7.91e^{-2} & -1.93e^{+3} & 0.00e^{+0} \\ -1.92e^{-1} & -1.32e^{-1} & 4.38e^{-1} & -5.34e^{-2} & -2.61e^{+2} & 0.00e^{+0} \\ 4.45e^{+0} & 3.36e^{-1} & -4.91e^{-1} & 8.87e^{-2} & 5.32e^{+3} & 0.00e^{+0} \\ 2.84e^{+1} & 2.22e^{+0} & -2.68e^{+0} & -1.89e^{+0} & 3.40e^{+4} & 0.00e^{+0} \\ \hline 6.38e^{-2} & -3.34e^{-1} & -3.72e^{-2} & -8.40e^{-3} & 0.00e^{+0} & -1.00e^{+3} \end{array}\right]$$

Acknowledgments

This experiment has been carried out jointly by the National Aerospace Laboratory and the National Space Development Agency supported by the Toshiba Corporation and the Mitsubishi Electric Corporation. The authors wish to gratefully acknowledge the engineers and researchers involved in this project.

References

[1]Grocott, S., How, J., Miller, D., MacMartin, D., and Liu, K., "Robust Control Design and Implementation on the Middeck Active Control Experiment," *Journal of Guidance, Control, and Dynamics*, Vol. 17, No. 6, 1994, pp. 1163–1170.

[2]Bukley, A. P., "Hubble Space Telescope Pointing Control System Design Improvement Study Results," *Journal of Guidance, Control, and Dynamics*, Vol. 18, No. 2, 1995, pp. 194–199.

[3]Kida, T., Yamaguchi, I., Ohkami, Y., Ichikawa, S., and Kawada Y., "A Flight Experiment of Flexible Spacecraft Attitude Control," 39th Congress of the International Astronautical Federation, IAF-Paper 88-044, Bangalore, India, Oct. 1988.

[4]Kida, T., Yamaguchi, I., Komatsu, K., Sano, M., Kasai, T., Suzuki, T., Ichikawa, S., Ishikawa, S., and Sekiguchi, T., "On-Orbit Flexible Structure Control Experiment of ETS-VI: Final Report of NAL/NASDA Joint Research," National Aerospace Lab., STR No. 8-9507, Tokyo, Japan, March 1996.

[5]Komatsu, K., Sano, M., Kai, T., Tsujihata, A., and Mitsuma, H., "Experimental Modal Analysis for Dynamics Models of Spacecraft," *Journal of Guidance, Control, and Dynamics*, Vol. 14, No. 3, 1991, pp. 686–688.

[6]Likins, P. W., "Dynamics and Control of Flexible Spacecraft," Jet Propulsion Lab., TR 32-1329, California Inst. of Technology, Pasadena, CA, Jan. 1970.

[7]Yamaguchi, I., Kida, T., and Kasai, T., "Experimental Demonstration of LSS System Identification," *Proceedings of American Control Conference* (Seattle, WA), American Automatic Control Council, Evanston, IL, 1995, pp. 407–411.

[8]Yamaguchi, I., Sekiguchi, T., Yamada, K., Chida, Y., and Adachi, S., "On-Orbit System Identification Experiment of ETS-VI," 11th International Astronautical Symposium, Gihu, Japan, May 1996, pp. 21–26.

[9]Anderson, B. D. O., and Moore, J. B., *Optimal Control*, Prentice–Hall, Englewood Cliffs, NJ, 1990, pp. 101–138.

[10]Anderson, B. D. O., and Mingori, D. L., "Use of Frequency Dependence in Linear Quadratic Control Problems to Frequency-Shape Robustness," *Journal of Guidance, Control, and Dynamics*, Vol. 8, No. 3, 1985, pp. 397–401.

[11]Kida, T., and Ikeda, M., "Robust Control for Large Space Structures," *Selected Papers from the International Federation of Automatic Control Symposium on Automatic Control in Aerospace* (Tsukuba, Japan), Pergamon, Oxford, England, UK, 1989, pp. 165–170.

[12]Kida, T., Tsubokawa, Y., and Ikeda, M., "Robust LSS Controller Design by Frequency Shaping," AIAA Paper 89-3535, July 1989.

[13]Franklin, G. F., Powell, J. D., and Emami-Naeini, A., *Feedback Control of Dynamic Systems*, Addison–Wesley, Reading, MA, 1991, pp. 418, 419.

[14]Maciejowski, J. M., *Multivariable Feedback Design*, Addison–Wesley, Wokingham, England, UK, 1989, pp. 265–324.

[15]Doyle, J., Glover, K., Khargonekar, P., and Francis, B., "State-Space Solutions to Standard H_2 and H_∞ Control Problems," *IEEE Transactions on Automatic Control*, Vol. 34, No. 8, 1989, pp. 831–841.

[16]Chiang, R., and Safonov, M., *Robust Control Toolbox User's Guide*, MathWorks, Natick, MA, 1992.

[17]Kimura, H., Oike, T., Miura, A., Akai, K., and Kida, T., "Robust Stability-Degree Assignment and Its Application to the Control of Flexible Structures," *International Journal of Robust and Nonlinear Control*, Vol. 1, 1991, pp. 153–169.

[18]Saeki, M., "H_∞ Control with Pole Assignment in a Specified Disk," *International Journal of Control*, Vol. 56, No. 3, 1922, pp. 725–731.

[19]Balas, M. J., "Direct Velocity Feedback Control of Large Space Structures," *Journal of Guidance and Control*, Vol. 2, No. 3, 1979, p. 252, 253.

[20]Joshi, S. M., "Robustness Properties of Collocated Controllers for Flexible Spacecraft," *Journal of Guidance, Control, and Dynamics*, Vol. 9, No. 1, 1986, pp. 85–91.

[21]Ikeda, M., Koujitani, K., and Kida, T., "Optimality of the Direct Velocity and Displacement Feedback for Large Space Structures with Collocated Sensors and Actuators," 12th International Federation of Automatic Control, World Congress, WE-A-4, Sydney, Australia, July 1993.